catalysts

MDPI

Article

Visible Light Induced Nano-Photocatalysis Trimetallic $Cu_{0.5}Zn_{0.5}$-Fe: Synthesis, Characterization and Application as Alcohols Oxidation Catalyst

Asma Ghazzy [1], Lina Yousef [2] and Afnan Al-Hunaiti [2,*]

[1] Faculty of Pharmacy, Al-Ahliyya Amman University, Amman 19328, Jordan; a.alghazzy@ammanu.edu.jo
[2] Department of Chemistry, The University of Jordan, Amman 11942, Jordan
* Correspondence: a.alhunaiti@ju.edu.jo

Abstract: Here, we report a visible light-induced-trimetallic catalyst ($Cu_{0.5}Zn_{0.5}Fe_2O_4$) prepared through green synthesis using *Tilia* plant extract. These nanomaterials were characterized for structural and morphological studies using powder x-ray diffraction (P-XRD), scanning electron microscopy (SEM) and thermogravimetric analysis (TGA). The spinel crystalline material was ~34 nm. In benign reaction conditions, the prepared photocatalyst oxidized various benzylic alcohols with excellent yield and selectivity toward aldehyde with 99% and 98%; respectively. Aromatic and aliphatic alcohols (such as furfuryl alcohol and 1-octanol) were photo-catalytically oxidized using $Cu_{0.5}Zn_{0.5}Fe_2O_4$, LED light, H_2O_2 as oxidant, 2 h reaction time and ambient temperature. The advantages of the catalyst were found in terms of reduced catalyst loading, activating catalyst using visible light in mild conditions, high conversion of the starting material and the recyclability up to 5 times without loss of the selectivity. Thus, our study offers a potential pathway for the photocatalytic nanomaterial, which will contribute to the advancement of photocatalysis studies.

Keywords: trimetallic; nanoparticles; iron oxide; photocatalytic; magnetic; alcohol; oxidation

Citation: Ghazzy, A.; Yousef, L.; Al-Hunaiti, A. Visible Light Induced Nano-Photocatalysis Trimetallic $Cu_{0.5}Zn_{0.5}$-Fe: Synthesis, Characterization and Application as Alcohols Oxidation Catalyst. *Catalysts* **2022**, *12*, 611. https://doi.org/10.3390/catal12060611

Academic Editors: Stéphanie Lambert and Julien Mahy

Received: 11 April 2022
Accepted: 27 May 2022
Published: 2 June 2022

1. Introduction

The high demand to use renewable energy sources is required to reduce the dependency on fossil fuels and the possibility to reduce emissions in the atmosphere. Therefore, solar energy can be a good renewable alternative to fossil fuels. In recent years, nano semiconductor photocatalysis, as a "green" technology, has been widely used for conducting various applications. Outstanding stability, good photostability, nontoxicity and low price make spinel iron oxide the photocatalyst of choice for environmental remediation [1–4]. It is known that the UV region occupies only ~4% of the entire solar spectrum, while 45% of the energy belongs to visible light [5]. Therefore, developing efficient visible-light photocatalysts for environmental remediation has become an active research area in photocatalysis research [6–12]. In the photoelectric conversion process, the most important reaction involves hydroxyl ions on the semiconductor surface reacting with the holes, forming hydroxyl radicals (·OH), which is the main cause of the photocatalytic activity. The hydroxyl radical is a powerful, non-selective oxidant that can rapidly oxidize many organic compounds [13]. Many perovskite- or spinel-type complex oxides have been found to have selective visible-light-driven photoactivity using peroxides as oxidant. Among them, ferrites have also received considerable attention as magnetic nanoparticles (MNPs) with diverse applications metal oxides (e.g., Fe_2O_3, $ZnFe_2O_4$, $NiCo_2O_4$, $MnFe_2O_4$ and $BiFeO_3$), as it may show visible light photocatalytic alternative [14–19].

Trimetallic iron-based oxides possess attractive properties and widespread applications [20]. One of the essential applications of trimetallic NPs is catalysis [21–24]. The catalyst efficiency surges exponentially by increasing the number of coordination sites through a significant increase in the surface/volume ratio of NPs. Glucose oxidation

produces gluconic acid under mild conditions catalyzed by Ag/Au/Pd NPs [24]. The cyclization reaction between diazodicarbonyl compounds and oxalyl chloride was carried out through green AuFeAg catalyst to afford α,β- or β,β-dichloroenones [25]. Moreover, large-scale sensitive and selective organic transformations achieved using trimetallic NPs in various forms such as core/shell [23], alloys [24] and layer-by-layer [25].

The catalytic activity can be dependent on preparation methods, as it affects the morphology and physiochemical properties of the material. Therefore, several methods have been applied in preparation of multi-metallic NPs. Among the known methods, electrochemical synthesis, chemical and hydrothermal synthesis, coprecipitation, sol-gel, mechanical alloying and solvothermal technologies are main techniques utilized [26,27]. Here we use coprecipitation technique using a plant extract as a reducing agent instead of unnecessary reagents. Generally, natural product extracts obtained from bio-renewable sources have a great potential as reducing, stabilizing material as it contains polyphenolic, glycoside and flavonoid compounds. Furthermore, the waxy material in plant extract can help in preventing the aggregation of powder nanoparticles, thus it can be applied for the greener production of mono- and multi-metallic NPs [28,29].

Oxidation of benzyl alcohol to produce the must-need industrial intermediate benzaldehyde is a crucial process in the industry. Within the aldehyde family, benzaldehyde is an essential building block for many industrial products [30]. The attractive interest of benzyl alcohol and benzaldehyde in the research area is noticeable as increase of preparation protocols for benzaldehydes production in the last decade, as well its applications. The heterogeneous catalytic oxidation of aryl or alkyl alcohol to supply various worthy chemicals such as aldehydes or carboxylic acids has been endorsed beneficial over homogenous catalytic techniques due to their recoverable fashion and the help of eco-friendly conditions like the use of H_2O_2 or O_2 as mild oxidants [31–34].

Herein, we report a trimetallic iron oxide-based NPs, as green and affordable catalyst using phyto mediated extract (*Telia*) in preparation of $Cu_{0.5}Zn_{0.5}Fe_2O_4$ that was applied as a photo-induced oxidation catalyst of benzyl alcohols and aliphatic alcohols. As shown in Scheme 1, benzyl alcohol oxidation is presented, exploiting mild reaction conditions. The characterization of the synthesized nanoparticles has been carried out in detail, employing the Rietveld refinement method using XRD data, SEM and TGA images.

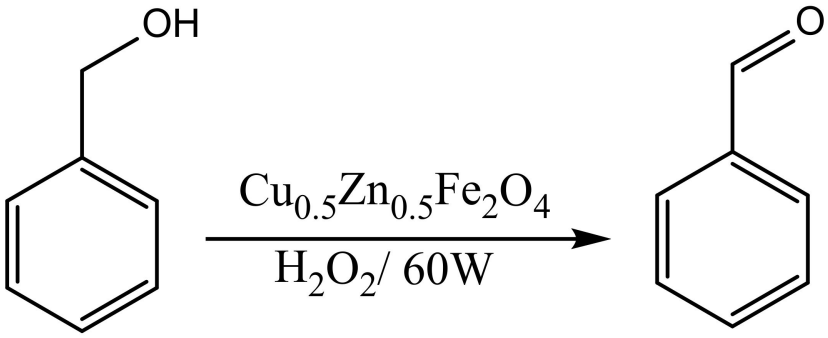

Scheme 1. Benzyl alcohol oxidation by using trimetallic Cu-Zn-Fe NPs in Acetonitrile.

To study the oxidation catalytic activity of Magnetic nanoparticles (MNP), benzyl alcohol was used as substrate model to optimize the reaction conditions. The present study has been extended to various alcohol substates to explore the possibilities of expanding the application of the catalyst, which shows a promising reactivity and applications. The novelty of the present work lies in the preparation of this magnetic trimetallic nanoparticles in a very simple, cheaper, eco-friendly coprecipitation synthesis process of nano particles, which can be used as a LED photo induced catalyst for oxidation of alcohols to obtain selectively aldehyde products.

2. Results and Discussion

2.1. Trimetallic Nanoparticles

The XRD patterns for the $Cu_{0.5}Zn_{0.5}FeO_4$ sample are shown in Figure 1. The XRD spectra for the samples with the diffraction peaks that appeared at 2θ values of 30.00, 35.40, 43.31, 50.41, 56.94 and 62.53 were assigned to the (220) (311) (400) (511) (440) and (550) planes, which was found to be in good agreement with $ZnFe_2O_4$ (PDF no. 01-089-1009) and Fe_3O_4 (PDF no. 01-088-0866). The signals consistent with the (220), (311), (400), (511), (440) and (533) reflect the spinel crystal structure of $CuFe_2O_4$ (PDF no.00-025-0283). These results show the successful loading of the cubic $Cu_{0.5}Zn_{0.5}$ Fe_2O_4 spinel ferrites structures JCPDS: JCPDS: 00-051-0386. The lattice constant and crystallite size of the nanoparticles have been deliberated from the most conspicuous peak (311) using the Scherrer formula [35]. The X-ray diffraction nanoparticles reveal that $Cu_{0.5}Zn_{0.5}Fe_2O_4$ NPs possess a single-phase major cubic (fcc) spinel. The experimentally perceived d arrangement values and proportional strengths agree with those described in the records.

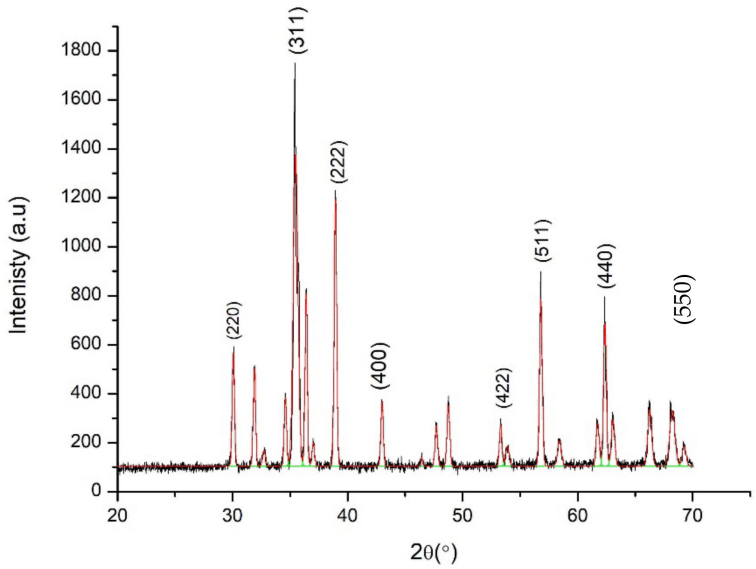

Figure 1. XRD patterns with Rietveld refinement the $Cu_{0.5}Zn_{0.5}Fe_2O_4$ sample.

The crystallite size (D) of each sample was calculated using the Stokes–Wilson Equation (1) [35,36]

$$D = \frac{\lambda}{\beta_c \cos\theta} \quad (1)$$

where λ is the X-ray wavelength, θ is the Bragg's angle of diffraction in degrees and β_c is the integral breadth of the diffraction peak corrected for the instrumental broadening. The diffraction peak used for the determination of the crystallite size was fitted with the relation:

$$\beta = \frac{A}{I_0} \quad (2)$$

Here A is the peak area and I_0 is the maximum intensity. The most intense peak (311) at 2θ = 35.6° was fitted to provide information regarding crystallite size in the direction perpendicular to the corresponding crystallographic plane. In addition, the size of spinel phase was determined with different crystallographic directions using the (220) reflection at 2θ = 30.0° and the (400) reflection at 43.04°; thus, the crystalline spinel $Cu_{0.5}Zn_{0.5}Fe_2O_4$ size was 34 nm.

The morphology of the prepared $CuZeFeO_4$ nanoparticles is explored by SEM image, as shown in Figure 2. The average particle size of the particles is ~31.2 nm.

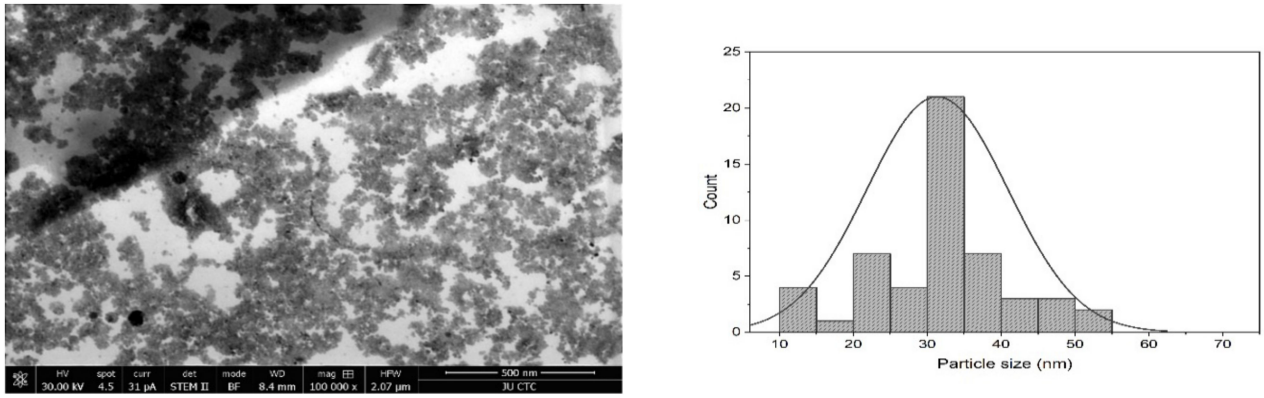

Figure 2. (**a**) FESEM images of the $Cu_{0.5}Zn_{0.5}Fe_2O_4$-NP; and (**b**) particle size distribution with a Gaussian fit average particle size (nm) = 31.2135 ± 0.23159.

2.2. TGA

Thermal stability of $Cu_{0.5}Zn_{0.5}Fe_2O_4$-NP was investigated by thermogravimetric analysis Figure 3. A gradual weight loss of 14 wt% was observed from 50–250 °C, owing to the reduction of water and CO_2 molecules [37]. In addition, the second drop of weight (12 wt%) at 250–450 °C can be attributed to the degradation of -OH ion from organic moieties of plant extract residues and decomposition of inorganic salts, which has two degradation mechanism involves both intermolecular and intramolecular transfer reactions [38]. The final loss of 11% occurred at 500–600 °C due to the formation of pure corresponding metal oxide. Notably, above 700 °C no weight loss was observed, which indicates the formation of $Cu_{0.5}Zn_{0.5}Fe_2O_4$-NP.

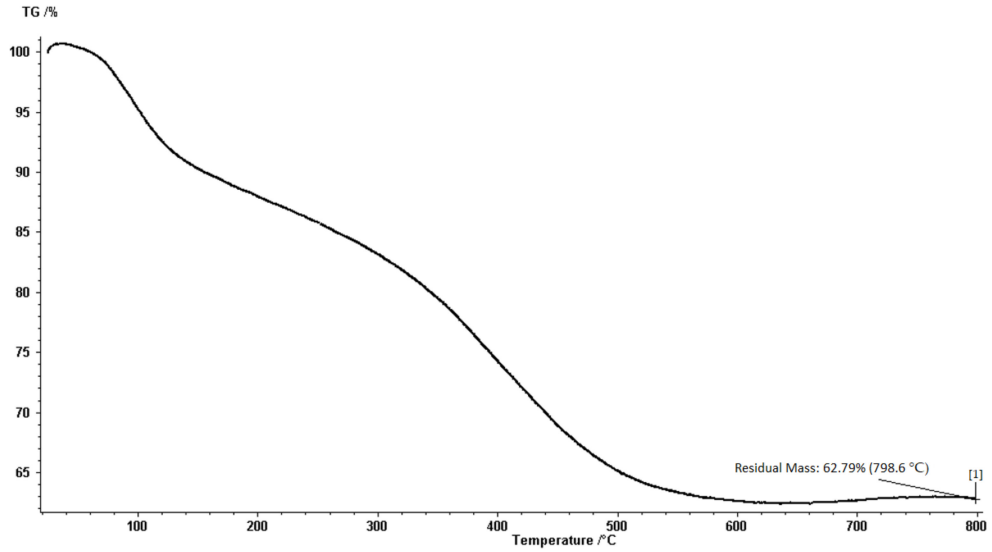

Figure 3. The thermogravimetric analysis (TGA) of the prepared nanoparticles.

2.3. Benzyl Alcohol Oxidation

The optimization of the catalytic reaction has been tested using benzyl alcohol as a model substrate, and the solvent effect is shown in Table 1. When using a different solvent, the reactivity changes drastically. To our delight, Acetonitrile has given the higher conversion for oxidizing benzyl alcohol (BA) into the anticipated aldehyde rather than isopropanol, while acetone and water have afforded a negligible amount of benzaldehyde. The high conversion of BA using acetonitrile can be explained via the formation of active radical species in the reaction media [39–41].

Table 1. Effect of solvents on the oxidation of benzyl alcohol.

Entry	Solvent	Yield * %
1	Acetonitrile	74
2	Isopropanol	67
3	Aceton	7
4	Water	2

* Benzaldehyde yield was analyzed using ^{1}H-NMR and UV-vis using internal standard. Reaction condition: benzyl alcohol = 0.1 mmol, catalyst = 15 mg, H_2O_2 = 250 mg, solvent 2 mL, light power 60 Watt, reaction time 4 h, temperature 25 °C.

In terms of optimizing reaction conditions, the influences of catalyst load amount, H_2O_2, on the BA substate have been shown in (Table 2). The blank experiments in entries 1 and 6 prove the need for catalyst and the oxidizing agent to produce an acceptable percentage of benzaldehyde. Excellent conversion (99%) of BA was obtained when the amount of catalyst load was 10–20 mg. Therefore, we used 10 mg of the catalyst to reduce the catalytic waste. Similarly, the H_2O_2 amount was optimized and 350 µL has provided the best targeted conversion into benzaldehyde. The role of the peroxide can be explained that the photo-induced electrons in the conduction band would dissolve oxygen and peroxide species which form peroxy and OH radicals intermediates. The reactive OH radicals species can oxidize alcohol into aldehyde.

Table 2. Quantitative optimization of Cu-Zn-Fe and oxidant amount.

Entry	Cu-Zn-Fe (mg)	H_2O_2 (µL)	Yield * %
1	0	350	1
2	7	350	95
3	10	350	99
4	15	350	99
5	20	350	89
6	10	0	9
7	10	250	54
8	10	350	99
9	10	500	99

* Benzaldehyde yield. Reaction condition: benzyl alcohol = 0.1 mmol, catalyst $Cu_{0.5}Zn_{0.5}Fe_2O_4$, ACN 2 mL, light power 60 Watt, reaction time 3 h, temperature 25 °C.

The effects of reaction time on the photocatalytic transformation of BA have been illustrated in Figure 4. The reaction was carried out up to 180 min, using the optimized conditions. In general, the oxidation rate of benzyl alcohol increased significantly when the reaction time raised for the first hour. The reaction ended up with a 99% yield in 120 min. This result shows that the catalyst is highly active in such conditions.

The catalytic performance is demonstrated by the four different illumination power from the LED source with an intensity of 7, 30, 60 and 120 W/cm^2, while the other conditions are set carefully at optimum conversion previous results. The reaction substrates included 10 mg of $Cu_{0.5}Zn_{0.5}Fe_2O_4$ catalyst, 1 mmol of benzyl alcohol, 350 mg of H_2O_2 and 2 mL of acetonitrile. With increasing illumination power by 23 W, the oxidation rate of benzyl alcohol surges dramatically to produce the highest yield 93%, while obviously the best conversion appears under 60 watt light power (Table 3).

Aliphatic and aromatic alcohol derivatives were chosen to explore the selective oxidation of various alcohol derivatives by $Cu_{0.5}Zn_{0.5}Fe_2O_4$ catalyst under the optimized conditions (Table 4). To our delight, the catalyst has shown a good to excellent reactivity toward both aliphatic and aromatic alcohols. Apparently, aromatic alcohols have shown high reactivity entries 1–4. The substituted benzylic alcohols have shown no effect on the obtained yield, while cinnamyl alcohol and the influence of allylic bond led to lower reactivity than the other aromatic substrates. This allows us to apply the catalyst to a lignin

substrate model such as furfuryl alcohol, and indeed the catalyst has excellent yield and selectivity.

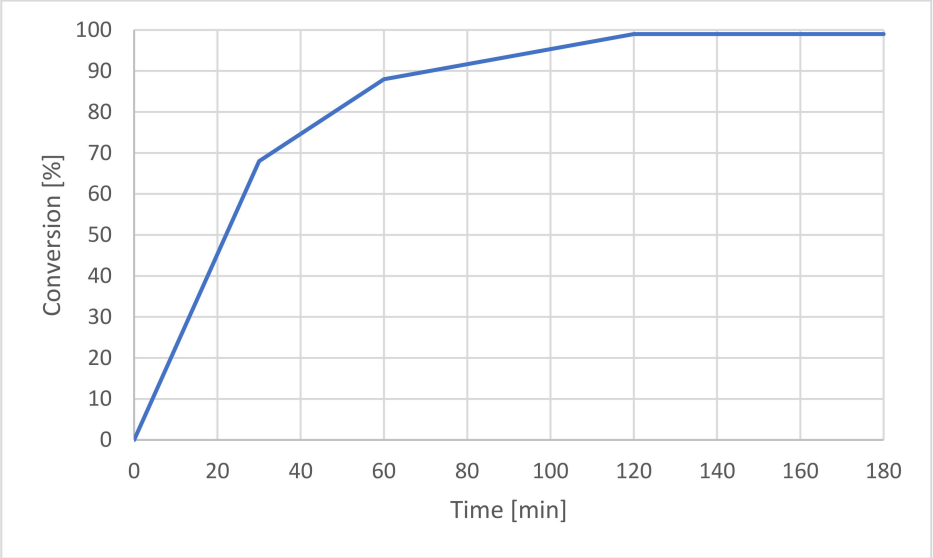

Figure 4. Effects of reaction time on the conversion of benzyl alcohol.

Table 3. Benzyl alcohol oxidation with different light power.

Entry	Light Power (W)	Yield * %
1	7	30.0
2	30	93.0
3	60	99
4	120	99

* Benzaldehyde yield. Reaction condition: (benzyl alcohol = 0.1 mmol, catalyst = 10 mg, Solvent ACN = 2 mL, H_2O_2 = 350 mg), reaction time 2 h, Temperature 25 °C.

Table 4. Alcohol derivatives on the selective oxidation of benzyl alcohol.

Entry	Substrate	Alcohol	Aldehyde	Yield * %
1	1-Octanol	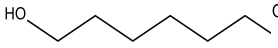	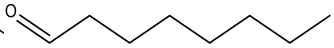	29.2
2	2-Octanol	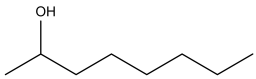	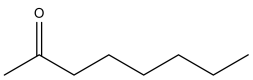	34.5
3	Furfuryl alcohol	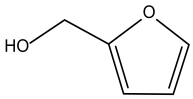	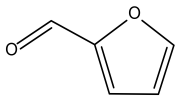	99
4	Cinnamyl alcohol	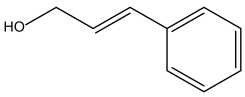	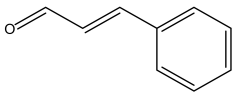	61.4
5	3,4-dimethyl benzyl alcohol	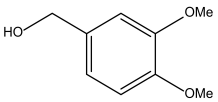	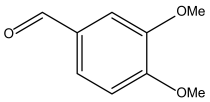	99
6	Benzyl alcohol	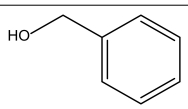	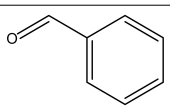	99

* Benzaldehyde yield. Reaction condition: (alcohol = 0.1 mmol, catalyst = 10 mg, Solvent ACN = 2 mL, H_2O_2 = 350 µL, light power 60 Watt, reaction time 2 h, Temperature 25 °C.

When comparing our results to previously reported results, several studies conveyed to prepare adequate metallic catalysts to achieve this transformation, when most of them either use expensive metals like Pd, Pt and Rh [42–44] or electrical sources [45], while the reaction conditions depend on intense light power between 150 to 450 W, or high temperature 80 to 120 °C in both natural and synthetic sources. In addition, the percentage yield of benzaldehyde varies widely from around 28 to 99, shown in Table 5.

Table 5. A comparison studies using di- and trimetallic NPs as catalyst to oxidize alcohols.

Source	Metallic NPs	Reaction Conditions	Conversion %	Selectivity %	Ref.
Synthatic	Au-Pd/O-CNTs	2 h, 120 °C, Solvent free	28.3	96	[42]
Synthatic	Au@Ag/BiOCl–OV	1 h, Xenon 300 W, CH_3CN	92	99	[43]
Synthatic	Trimetallic PtPbBi	Electrical	-	-	[44]
Synthatic	2.5% Au + 2.5% Pd/TiO_2DP2	140 °C, 10 bar O_2	84	40	[45]
Synthatic	Pd/$H_2Ti_3O_7$ Nanowires	Halogen 150 W, 90 °C	49.5	76	[46]
Synthatic	TiO_2	LED 450 W, 36 h, O_2	99	99	[47]
Nature *(Cacumen Platycladi)*	Au−Pd/TiO_2	6 h, 90 °C, O_2	74.2	98	[48]
Nature *(Oak fruit bark)*	Pd NPs	12 h, 80 °C, K_2CO_3	95	-	[49]
This work (*Tilia*)	Trimetallic Cu-Zn-Fe	2 h, LED 60 W, H_2O_2	99	99	

2.4. Recyclability

The stability of the prepared materials when exposed to consecutive reaction cycles was tested. Therefore, we examine the recyclability by using benzyl alcohol as a substrate in the presence of 10 mg of the catalyst.

The catalyst was reused up to four successive runs without drastic loss in activity. The catalyst was washed with water/ethanol solution and oven dried pre-use for oxidation of benzyl alcohol (Figure 5). Interestingly, after the 5th run, the weight loss of the catalyst was 28 wt% using gravimetric assay. The drop in the reactivity can be due to the slight deactivation of the catalyst via leaching some of the metals in the nanoparticles, or poising the catalyst surface of unwanted reaction products. After the fifth cycle, the conversion dropped slightly without any loss of selectivity.

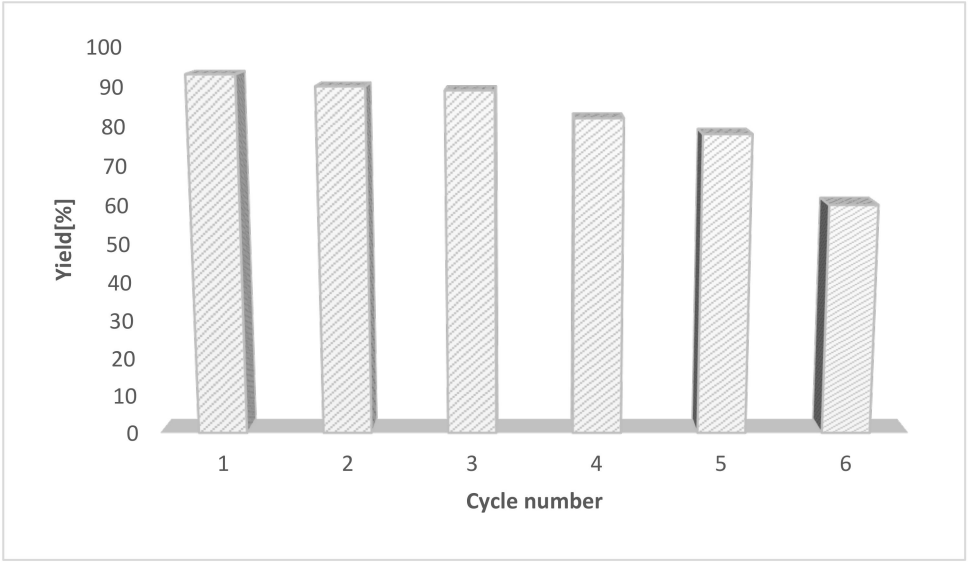

Figure 5. Recyclability test of $Cu_{0.5}Zn_{0.5}Fe_2O_4$-NP catalyst. The weight loss of catalyst after 5th runs was 28 wt%.

3. Experimental

3.1. Materials

The solvents used were purchased from sigma-Aldrich (Taufkirchen, Germany). $FeSO_4 \cdot 7H_2O$, $Zn(OAc)_2 \cdot 2H_2O$ $CuSO_4 \cdot 5H_2O$ and alcohols used were purchased from Sigma-Aldrich with 99.95% purity, and used as received. *Tilia* leaves extract was collected from a cultivated area in Amman, Jordan, during the flowering period in early spring of 2021. Sodium chloride (NaCl), acetic acid, sodium hydroxide and distilled water were used for all experiments. The crystallographic structure of MFe_2O_4 nano-ferrites was determined from the Powder X-ray diffraction (P-XRD, mnochromatic Cu-Kα radiation, nickel filter, 40 kV, 30 mA using Shimadzu XRD-7000, Japan) pattern, while the particle morphology and size distribution was determined with the aid of electron microscopy imaging (SEM, JOEL 6400 and FEI QUANTA 200, Japan).

3.2. Copper-Zinc Ferrite $Cu_{0.5}Zn_{0.5}Fe_2O_4$ NP Synthesis

The trimetallic ferrite nanoparticles were synthesized using an aqueous extract of *Telia*, as described previously [27]. Briefly, 1.12 g of $FeSO_4.7H_2O$ and 0.48 g of $Zn(OAC)_2.2H_2O$ and 0.48 g $CuSO_4 \cdot 5H_2O$ were dispersed in 20 mL distilled water for 1 h at room temperature under stirring, in order to obtain the homogeneous solution. A 50 mL of the aqueous plant extract was drop-wise added to the solution, and the mixture was stirred for 1 h and later the pH was controlled to obtain pH 10–12. The homogenous solution was then centrifuged, and the obtained solid products were collected and washed with distilled water and ethanol several times. Finally, the samples were dried in a vacuum oven at 60 °C for 6 h, and later calcinated at 1000 °C.

3.3. Characterization

The morphology and crystallinity of the synthesized $Cu_{0.5}Zn_{0.5}Fe_2O_4$ nanoparticles were determined via field emission scanning electron microscopy (SEM, FESEM JEOL JSM-6380) and (XRD, X'pert diffractometer using CuK α radiation), respectively. All measurements were performed at room temperature (25 $\pm$ 2 °C). Thermogravimetric analysis was accomplished using the System Setaram Setsys 12 TGA instrument (Setaram Instrumentation, Caluire, France), by heating the sample up to 800 °C at a rate of 10 °C·min^{-1}.

3.4. Photocatalytic Oxidation of Benzyl Alcohol to Benzaldehyde

To a stirred solution of 2 mL of acetonitrile containing 0.1 mmol benzyl alcohol, 15 mg of the prepared catalyst and 350 µL of H_2O_2 was added drop wise pre-irradiation. Subsequently, the suspension was irradiated by a 60 W LED, and the reaction was monitored by the absorbance using UV-vis for each sample.

3.5. Product Analysis

When the reaction ended, the magnetic catalyst was removed by applying an external magnet and the product was extracted by column chromatography and analyzed by ^{1}H-NMR and compared to the commercially available chemicals. The conversion percentage of benzyl alcohol was calculated by using the following Equation (3)

$$\text{Conversion (\%)} = [(C_0 - C_r)/C_0] \times 100\% \quad (3)$$

where C_0 is the initial concentration of benzyl alcohol and C_r and C_t are the concentrations of benzyl alcohol and benzaldehyde, respectively.

3.6. Experimental Procedure for the Reuse of the Catalyst

The reaction was applied for benzyl alcohol oxidation in a 1.0 mmol scale. Keeping reaction conditions constant, except using the recycled $Cu_{0.5}Zn_{0.5}Fe_2O_4$ catalyst rather than fresh catalyst, the reaction was monitored. When the reaction ended, the catalyst was removed using an external magnet and the product was analyzed by either ^{1}H-NMR or

UV-Vis. The catalyst was collected and washed with water/ethanol (5 mL) three times and oven dried pre-reuse. The dried catalyst was applied for further catalytic cycle up to 5 times without any severe loss of reactivity.

4. Conclusions

In this study, we synthesized phyto-mediated trimetallic Np of $Cu_{0.5}Zn_{0.5}Fe_2O_4$ using a Telia extract. The NP catalyst was characterized by powder XRD, FESEM and TGA studies. The XRD indicated a spinel ferrite with average crystalline diameter ~34 nm and average particle size of 31.2 nm by the SEM. The trimetallic nanoparticles has great potential to act as a visible light photocatalyst using LED light for the oxidation of benzylic and aliphatic alcohols selectively to aldehyde, with high selectivity and reactivity under benign reaction conditions using 10 mg of catalyst, 3 equivalent H_2O_2, 60 W light and 2 h reaction time. Later, the catalyst was compared to previous works, and it shows a promising reactivity. The novelty of this study lies in the preparation of the magnetic trimetallic nanoparticles in a very simple, cheap and eco-friendly coprecipitation synthesis process of nano particles, which offers a potential pathway for photocatalytic oxidation reaction.

Author Contributions: Conceptualization, A.A.-H.; methodology, A.A.-H. and A.G.; software, L.Y. and A.A.-H.; validation, A.A.-H. and A.G.; formal analysis, A.A.-H. and L.Y.; investigation, A.G. and A.A.-H.; resources, A.A.-H.; writing—original draft preparation, A.G. and A.A.-H.; writing—review and editing, A.A.-H. and A.A.-H.; visualization, A.G. and A.A.-H.; supervision, A.A.-H.; project administration, A.A.-H.; and funding acquisition, A.A.-H. All authors have read and agreed to the published version of the manuscript.

Funding: This research was supported by Deanship of Academic Research at the University of Jordan (Grant No. 2364), and Al-Ahliyya Amman University.

Data Availability Statement: Not applicable.

Acknowledgments: The Jordanian Cell Therapy Center (CTC) is acknowledged for the SEM imaging. A.A.-H. acknowledges support by the Deanship of Scientific Research at the University of Jordan. A.G. would like to acknowledges support by Deanship of Scientific Research at Al-Ahliyya Amman University.

Conflicts of Interest: The authors declare no conflict of interest.

References

1. Ng, Y.H.; Lightcap, I.V.; Goodwin, K.; Matsumura, M.; Kamat, P.V. To What Extent Do Graphene Scaffolds Improve the Photovoltaic and Photocatalytic Response of TiO_2 Nanostructured Films? *J. Phys. Chem. Lett.* **2010**, *1*, 2222–2227. [CrossRef]
2. Zhang, H.; Lv, X.; Li, Y.; Wang, Y.; Li, J. P25-graphene Composite as a High Performance Photocatalyst. *ACS Nano* **2010**, *4*, 380–386. [CrossRef] [PubMed]
3. Woan, K.; Pyrgiotakis, G.; Sigmund, W. Photocatalytic Carbon Nanotube TiO_2 Composites. *Adv. Mater.* **2009**, *21*, 2233–2239. [CrossRef]
4. Kumaresan, L.; Mahalakshmi, M.; Palanichamy, M.; Murugesan, V. Synthesis, Characterization, and Photocatalytic Activity of Sr2þ Doped TiO_2 Nanoplates. *Ind. Eng. Chem. Res.* **2010**, *49*, 1480–1485. [CrossRef]
5. Zhang, Z.J.; Wang, W.Z.; Yin, W.Z.; Shang, M.; Wang, L.; Sun, S.M. Inducing Photocatalysis by Visible Light Beyond the Absorption Edge: Effect of Upconversion Agent on the Photocatalytic Activity of Bi_2WO_6. *Appl. Catal. B* **2010**, *101*, 68–73. [CrossRef]
6. Liang, Y.Y.; Wang, H.L.; Casalongue, H.S.; Chen, Z.; Dai, H.J. TiO_2 Nanocrystals Grown on Graphene as Advanced Photocatalytic Hybrid Materials. *Nano Res.* **2010**, *3*, 701–705. [CrossRef]
7. Vijayan, B.K.; Dimitrijevic, N.M.; Wu, J.S.; Gray, K.A. The Effects of Pt Doping on the Structure and Visible Light Photoactivity of Titania Nanotubes. *J. Phys. Chem. C* **2010**, *114*, 21262–21269. [CrossRef]
8. Romcevic, N.; Kostic, R.; Hazic, B.; Romcevic, M.; KuryliszynKudelska, I.; Dobrowolski, W.D.; Narkiewicz, U.; Sibera, D. Raman Scattering from ZnO Incorporating Fe Nanoparticles: Vibrational Modes and Low-Frequency Acoustic Modes. *J. Alloys Compd.* **2010**, *507*, 386–390. [CrossRef]
9. Cai, L.; Liao, X.; Shi, B. Using Collagen Fiber as a Template to Synthesize TiO_2 and Fex/TiO_2 Nanofibers and Their Catalytic Behaviors on the Visible Light-Assisted Degradation of Orange II. *Ind. Eng. Chem. Res.* **2010**, *49*, 3194–3199. [CrossRef]
10. Guo, R.Q.; Fang, L.A.; Dong, W.; Zheng, F.G.; Shen, M.R. Enhanced Photocatalytic Activity and Ferromagnetism in Gd Doped $BiFeO_3$ Nanoparticles. *J. Phys. Chem. C* **2010**, *114*, 21390–21396. [CrossRef]

11. Cai, W.D.; Chen, F.; Shen, X.X.; Chen, L.J.; Zhang, J.L. Enhanced Catalytic Degradation of AO_7 in the CeO_2-H_2O_2 System with Fe3þ Doping. *Appl. Catal. B* **2010**, *101*, 160–168. [CrossRef]
12. Shu, X.; He, J.; Chen, D. Visible-Light-Induced Photocatalyst Based on Nickel Titanate Nanoparticles. *Ind. Eng. Chem. Res.* **2008**, *47*, 4750–4753. [CrossRef]
13. Hirakawa, T.; Nosaka, Y. Properties of O_2 and OH Formed in TiO_2 Aqueous Suspensions by Photocatalytic Reaction and the Influence of H_2O_2 and Some Ions. *Langmuir* **2002**, *18*, 3247–3325. [CrossRef]
14. Xu, S.H.; Feng, D.L.; Shangguan, W.F. Preparations and Photocatalytic Properties of Visible-Light-Active Zinc Ferrite-Doped TiO_2 Photocatalyst. *J. Phys. Chem. C* **2009**, *113*, 2463–2467. [CrossRef]
15. Laokul, P.; Amornkitbamrung, V.; Seraphin, S.; Maensiri, S. Characterization and Magnetic Properties of Nanocrystalline $CuFe_2O_4$, $NiFe_2O_4$, $ZnFe_2O_4$ Powders Prepared by the Aloe Vera Extract Solution. *Curr. Appl. Phys.* **2011**, *11*, 101–108. [CrossRef]
16. Zhang, B.P.; Zhang, J.L.; Chen, F. Preparation and Characterization of Magnetic $TiO_2/ZnFe_2O_4$ Photocatalysts by a sol-gel Method. *Res. Chem. Intermed.* **2008**, *34*, 375–380. [CrossRef]
17. Gómez-Pastora, J.; Bringas, E.; Ortiz, I. Recent progress and future challenges on the use of high performance magnetic nano-adsorbents in environmental applications. *Chem. Eng. J.* **2014**, *256*, 187–204. [CrossRef]
18. Al-Hunaiti, A.; Ghazzy, A.; Sweidan, N.; Mohaidat, Q.; Bsoul, I.; Mahmood, S.; Hussein, T. Nano-Magnetic $NiFe_2O_4$ and Its Photocatalytic Oxidation of Vanillyl Alcohol—Synthesis, Characterization, and Application in the Valorization of Lignin. *Nanomaterials* **2021**, *11*, 1010. [CrossRef]
19. Al-Hunaiti, A.; Mohaidat, Q.; Bsoul, I.; Mahmood, S.; Taher, D.; Hussein, T. Synthesis and characterization of novel phyto-mediated catalyst, and its application for a selective oxidation of (VAL) into vanillin under visible light. *Catalysts* **2020**, *10*, 839. [CrossRef]
20. Sharma, G.; Kumar, D.; Kumar, A.; Ala'a, H.; Pathania, D.; Naushad, M.; Mola, G.T. Revolution from monometallic to trimetallic nanoparticle composites, various synthesis methods and their applications: A review. *Mater. Sci. Eng. C* **2017**, *71*, 1216–1230. [CrossRef]
21. Mondal, B.N.; Basumallick, A.; Chattopadhyay, P.P. Magnetic behavior of nanocrystalline Cu–Ni–Co alloys prepared by mechanical alloying and isothermal annealing. *J. Alloys Compd.* **2008**, *457*, 10–14. [CrossRef]
22. Roshanghias, A.; Bernardi, J.; Ipser, H. An attempt to synthesize Sn-Zn-Cu alloy nanoparticles. *Mater. Lett.* **2016**, *178*, 10–14. [CrossRef]
23. Lan, J.; Li, C.; Liu, T.; Yuan, Q. One-step synthesis of porous PtNiCu trimetallic nanoalloy with enhanced electrocatalytic performance toward methanol oxidation. *J. Saudi Chem. Soc.* **2019**, *23*, 43–51. [CrossRef]
24. Venkatesan, P.; Santhanalakshmi, J. Designed synthesis of Au/Ag/Pd trimetallic nanoparticle-based catalysts for Sonogashira coupling reactions. *Langmuir* **2010**, *26*, 12225–12229. [CrossRef]
25. Duan, H.; Wang, D.; Li, Y. Green chemistry for nanoparticle synthesis. *Chem. Soc. Rev.* **2015**, *44*, 5778–5792. [CrossRef]
26. Iravani, S.; Varma, R. Plant-derived Edible Nanoparticles and miRNAs: Emerging Frontier for Therapeutics and Targeted Drug-delivery. *ACS Sustain. Chem. Eng.* **2019**, *7*, 8055–8069. [CrossRef]
27. Imraish, A.; Al-Hunaiti, A.; Abu-Thiab, T.; Ibrahim, A.; Hwaitat, E.; Omar, A. Phyto-Facilitated Bimetallic $ZnFe_2O_4$ Nanoparticles via *Boswellia carteri*: Synthesis, Characterization, and Anti-Cancer Activity. *Anti-Cancer Agents Med. Chem.* **2021**, *21*, 1767–1772. [CrossRef]
28. Iravani, S.; Varma, R.S. Plants and plant-based polymers as scaffolds for tissue engineering. *Green Chem.* **2019**, *21*, 4839–4867. [CrossRef]
29. Pugh, S.; McKenna, R.; Halloum, I.; Nielsen, D.R. Engineering *Escherichia coli* for Renewable Benzyl Alcohol Production. *Metab. Eng. Commun.* **2015**, *2*, 39–45. [CrossRef]
30. Pillai, U.R.; Sahle-Demessie, E. Oxidation of alcohols over Fe^{3+}/montmorillonite-K10 using hydrogen peroxide. *Appl. Catal. A-Gen.* **2003**, *245*, 103–109. [CrossRef]
31. O'Brien, P.; Lopez-Tejedor, D.; Benavente, R.; Palomo, J.M. Pd Nanoparticles-Polyethylenemine-Lipase Bionanohybrids as Heterogeneous Catalysts for Selective Oxidation of Aromatic Alcohols. *ChemCatChem* **2018**, *10*, 4992–4999. [CrossRef]
32. Alshammari, H.M.; Alshammari, A.S.; Humaidi, J.R.; Alzahrani, S.A.; Alhumaimess, M.S.; Aldosari, O.F.; Hassan, H. Au-Pd Bimetallic Nanocatalysts Incorporated into Carbon Nanotubes (CNTs) for Selective Oxidation of Alkenes and Alcohol. *Processes* **2020**, *8*, 1380. [CrossRef]
33. An, H.; Deng, C.; Sun, Y.; Lv, Z.; Cao, L.; Xiao, S.; Zhao, L.; Yin, Z. Design of Au@ Ag/BiOCl–OV photocatalyst and its application in selective alcohol oxidation driven by plasmonic carriers using O_2 as the oxidant. *CrystEngComm* **2020**, *22*, 6603–6611. [CrossRef]
34. Smit, J.; Wijn, H.P.J.; Ferrites; Mahmood, S.H. Properties and Synthesis of Hexaferrites. In *Hexaferrite Permanent Magnetic Material*; Wiley: New York, NY, USA, 1959; p. 54.
35. Mahmood, S.H. Magnetic anisotropy in fine magnetic particles. *J. Magn. Magn. Mater.* **1993**, *118*, 359–364. [CrossRef]
36. Narayanasamy, A.; Jeyadevan, B.; Chinnasamy, C.N.; Ponpandian, N.; Greneche, J.M. Structural, magnetic and electrical properties of spinel ferrite nanoparticles. In Proceedings of the Ninth International Conference on Ferrites, San Francisco, CA, USA, 3 January 2005; pp. 867–875.
37. Rincón-Granados, K.L.; Vázquez-Olmos, A.R.; Vega-Jiménez, A.; Ruiz, F.; Garibay-Febles, V.; Ximénez-Fyvie, L. Preparation, characterization and photocatalytic activity of NiO, Fe_2O_3 and $NiFe_2O_4$. *Materialia* **2021**, *15*, 177–182.

38. Marmisollé, W.A.; Azzaroni, O. Recent developments in the layer-by-layer assembly of polyaniline and carbon nanomaterials for energy storage and sensing applications. From synthetic aspects to structural and functional characterization. *Nanoscale* **2016**, *8*, 9890–9918. [CrossRef]
39. Jiang, C.; Markutsya, S.; Tsukruk, V.V. Compliant, robust, and truly nanoscale free-standing multilayer films fabricated using spin-assisted layer-by-layer assembly. *Adv. Mater.* **2004**, *16*, 157–161. [CrossRef]
40. Kroschwitz, J.I.; Howe-Grant, M. *Kirk-Othmer Encyclopedia of Chemical Technology*; John Wiley and Sons: New York, NY, USA, 1991; p. 127.
41. Al-Hunaiti, A.; Al-Said, N.; Halawani, L.; Haija, M.A.; Baqaien, R.; Taher, D. Synthesis of magnetic $CuFe_2O_4$ nanoparticles as green catalyst for toluene oxidation under solvent-free conditions. *Arab. J. Chem.* **2020**, *13*, 4945–4953. [CrossRef]
42. Karimi, B.; Abedi, S.; Clark, J.; Budarin, V. Highly efficient aerobic oxidation of alcohols using a recoverable catalyst: The role of mesoporous channels of SBA-15 in stabilizing palladium nanoparticles. *Angew. Chem. Int. Ed.* **2006**, *17*, 4776–4779. [CrossRef]
43. Wang, C.; Chen, W.; Chang, H.T. Enzyme Mimics of Au/Ag Nanoparticles for Fluorescent Detection of Acetylcholine. *Anal. Chem.* **2012**, *84*, 9706–9712. [CrossRef]
44. Zhu, Z.; Liu, F.; Fan, J.; Li, Q.; Min, Y.; Xu, Q. C_2 Alcohol Oxidation Boosted by Trimetallic PtPbBi Hexagonal Nanoplates. *ACS Appl. Mater. Interfaces* **2020**, *12*, 52731–52740. [CrossRef] [PubMed]
45. Miedziak, P.; Sankar, M.; Dimitratos, N.; Lopez-Sanchez, J.A.; Carley, A.F.; Knight, D.W.; Brian, T.; Christopher, J.K.; Hutchings, G.J. Oxidation of benzyl alcohol using supported gold–palladium nanoparticles. *Catal. Today* **2011**, *164*, 315–319. [CrossRef]
46. Higashimoto, S.; Kitao, N.; Yoshida, N.; Sakura, T.; Azuma, M.; Ohue, H.; Sakata, Y. Selective photocatalytic oxidation of benzyl alcohol and its derivatives into corresponding aldehydes by molecular oxygen on titanium dioxide under visible light irradiation. *J. Catal.* **2009**, *266*, 279–285. [CrossRef]
47. Du, M.; Zeng, G.; Huang, J.; Sun, D.; Li, Q.; Wang, G.; Li, X. Green photocatalytic oxidation of benzyl alcohol over noble-metal-modified $H_2Ti_3O_7$ nanowires. *ACS Sustain. Chem. Eng.* **2019**, *7*, 9717–9726. [CrossRef]
48. Hong, Y.; Jing, X.; Huang, J.; Sun, D.; Odoom-Wubah, T.; Yang, F.; Li, Q. Biosynthesized bimetallic Au–Pd nanoparticles supported TiO_2 for solvent-free oxidation of benzyl alcohol. *ACS Sustain. Chem. Eng.* **2014**, *2*, 1752–1759. [CrossRef]
49. Veisi, H.; Hemmati, S.; Qomi, M. Aerobic oxidation of benzyl alcohols through biosynthesized palladium nanoparticles mediated by Oak fruit bark extract as an efficient heterogeneous nanocatalyst. *Tetrahedron Lett.* **2017**, *58*, 4191–4496. [CrossRef]